LETTER

doi:10.1038/nature15529

Diversion of aspartate in ASS1-deficient tumours fosters *de novo* pyrimidine synthesis

Shiran Rabinovich[1]*, Lital Adler[1]*, Keren Yizhak[2], Alona Sarver[1], Alon Silberman[1], Shani Agron[1], Noa Stettner[1], Qin Sun[3], Alexander Brandis[4], Daniel Helbling[5], Stanley Korman[6], Shalev Itzkovitz[7], David Dimmock[5], Igor Ulitsky[1], Sandesh C. S. Nagamani[3,8], Eytan Ruppin[2,9,10] & Ayelet Erez[1]

Cancer cells hijack and remodel existing metabolic pathways for their benefit. Argininosuccinate synthase (ASS1) is a urea cycle enzyme that is essential in the conversion of nitrogen from ammonia and aspartate to urea. A decrease in nitrogen flux through ASS1 in the liver causes the urea cycle disorder citrullinaemia[1]. In contrast to the well-studied consequences of loss of ASS1 activity on ureagenesis, the purpose of its somatic silencing in multiple cancers is largely unknown[2]. Here we show that decreased activity of ASS1 in cancers supports proliferation by facilitating pyrimidine synthesis via CAD (carbamoyl-phosphate synthase 2, aspartate transcarbamylase, and dihydroorotase complex) activation. Our studies were initiated by delineating the consequences of loss of ASS1 activity in humans with two types of citrullinaemia. We find that in citrullinaemia type I (CTLN I), which is caused by deficiency of ASS1, there is increased pyrimidine synthesis and proliferation compared with citrullinaemia type II (CTLN II), in which there is decreased substrate availability for ASS1 caused by deficiency of the aspartate transporter citrin. Building on these results, we demonstrate that ASS1 deficiency in cancer increases cytosolic aspartate levels, which increases CAD activation by upregulating its substrate availability and by increasing its phosphorylation by S6K1 through the mammalian target of rapamycin (mTOR) pathway. Decreasing CAD activity by blocking citrin, the mTOR signalling, or pyrimidine synthesis decreases proliferation and thus may serve as a therapeutic strategy in multiple cancers where *ASS1* is downregulated. Our results demonstrate that *ASS1* downregulation is a novel mechanism supporting cancerous proliferation, and they provide a metabolic link between the urea cycle enzymes and pyrimidine synthesis.

In contrast to the well-delineated biochemical and clinical consequences of loss-of-function germline mutations in *ASS1*, which have not been reported to include cancer, studies have shown a correlation between somatic deficiency of ASS1 in cancer and poor prognosis, for which the mechanism remains obscure[2,3]. Outside the liver, ASS1 is expressed in most tissues where it catalyses the penultimate step in the synthesis of arginine. Argininosuccinate lyase (ASL), the enzyme downstream of ASS1, is directly responsible for arginine synthesis[4] (Fig. 1a). A well-established sequel of ASS1 and/or ASL deficiency is arginine auxotrophy[5]; thus, arginine-catabolizing enzymes have been used as therapy in ASS1-depleted tumours with limited benefit, especially in melanoma, wherein the cancer cells develop resistance by re-expressing ASS1 within days[3]. Since there are cancers in which both these genes are epigenetically silenced[6], ASS1 deficiency in cancers might have an arginine-independent effect, which may be related to its substrate, aspartate (Fig. 1a).

In the cytosol, aspartate serves as a substrate both for ASS1 and for the enzymatic complex CAD. We thus hypothesized that decreased ASS1 activity might enhance aspartate availability for CAD for the synthesis of pyrimidine nucleotides to promote proliferation (Fig. 1a). If correct, deficiency in the mitochondrial aspartate transporter, citrin, would be expected to decrease aspartate availability both for ASS1 and for CAD and hence restrict proliferation (Fig. 1a).

We first assessed the correlation between ASS1 levels and proliferation in non-cancerous states. A generic stoichiometric model of human metabolism[7] predicted that inactivation of ASS1 is significantly associated with an increase in growth rate, and is additionally predicted to increase flux through the reaction catalysed by CAD (Fig. 1b). Thus, we expected subjects with ASS1 deficiency (CTLN I) to have increased synthesis of pyrimidines owing to increased utilization of aspartate by CAD, compared with those with CTLN II in whom aspartate availability to CAD is decreased (Fig. 1a). Indeed, urinary levels of orotic acid, a product reflecting the synthetic activity of CAD, were significantly elevated in human subjects with CTLN I compared with the normative values from a control population and with subjects with CTLN II (Fig. 1a, c). Moreover, we found that CTLN I fibroblasts have increased synthesis of pyrimidines and proliferation compared with CTLN II cells (Fig. 1d, e). Using [$^{15}N_5$]α-glutamine we further showed that CTLN I cells generate more total as well as labelled M + 1 aspartate and M + 1 uracil, compared with control and CTLN II fibroblasts (Fig. 1f, g and Extended Data Fig. 1a–c). Hence, there is a specific decrease in aspartate transport from the mitochondria in CTLN II, leading to reduced aspartate availability for pyrimidine synthesis and restricting proliferation. Interestingly, growth restriction has been reported in humans with CTLN II[8] but no growth aberrancies have been reported in CTLN I, further providing a clinical human context to the findings and suggesting that, in physiological proliferation, aspartate deficiency has more severe clinical consequences than its enrichment. To corroborate our results in another model system, we analysed *Ass1* messenger RNA (mRNA) levels in wild-type newborn mouse intestines, which express high levels of Ass1 and contain proliferating and differentiated cells in the crypts and villi, respectively[9]. We found a significant correlation between the levels of *Ass1* and *Glut2*, a mature enterocyte marker in the differentiated enterocytes in the villi, whereas a significant inverse correlation was observed between *Ass1* and *Ki67*, a marker of proliferation, in the proliferating cells in the crypts (Fig. 1h). Thus, ASS1 inactivation has an important role in proliferation of non-cancerous cells, by increasing aspartate availability for pyrimidine synthesis by CAD.

We next evaluated whether this mechanism could be the reason for the downregulation of *ASS1* in cancer. According to the well-established 'Warburg effect', different metabolites are diverted from

[1]Department of Biological Regulation, Weizmann Institute of Science, Rehovot 7610001, Israel. [2]The Blavatnik School of Computer Science, Tel Aviv University, Tel Aviv 69978, Israel. [3]Department of Molecular and Human Genetics, Baylor College of Medicine, Houston, Texas 77030, USA. [4]Biological Services, Weizmann Institute of Science, Rehovot 69978, Israel. [5]Human and Molecular Genetic and Biochemistry Center, Medical College Wisconsin, Milwaukee, Wisconsin 53226, USA. [6]Genetic and Metabolic Center, Hadassah Medical Center, Jerusalem 91120, Israel. [7]Department of Molecular Cell Biology, Weizmann Institute of Science, Rehovot 69978, Israel. [8]Texas Children's Hospital, Houston, Texas 77030, USA. [9]The Sackler School of Medicine, Tel Aviv University, Tel Aviv 69978, Israel. [10]Center for Bioinformatics and Computational Biology & Department of Computer Science, University of Maryland, College Park, Maryland 20742, USA.
*These authors contributed equally to this work.

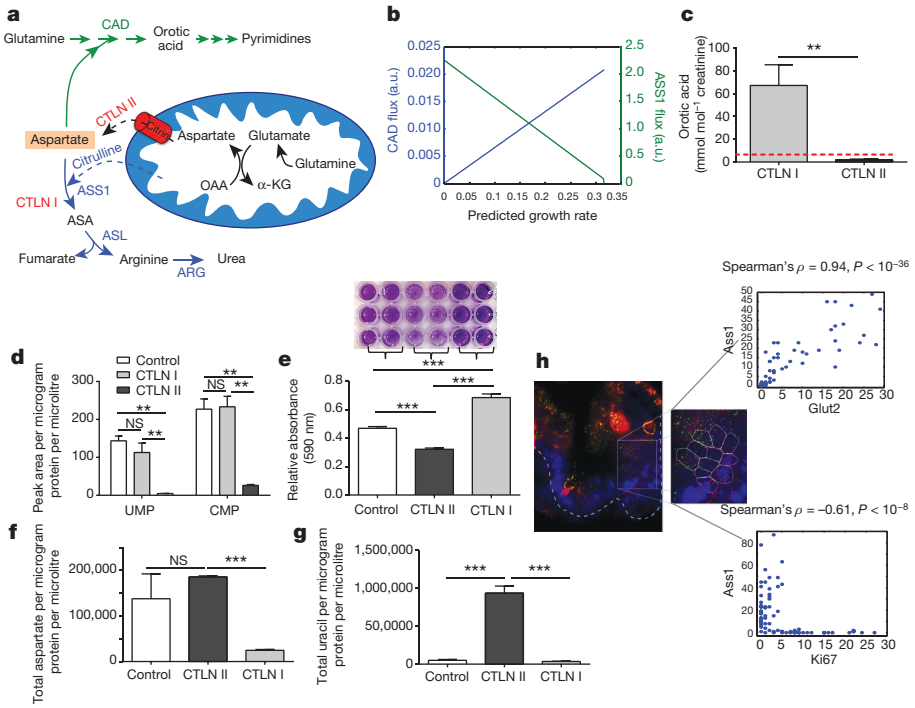

Figure 1 | ASS1 inactivation correlates with non-cancerous proliferation. a, Illustration of the metabolic flux involved in nitrogen contributions to nucleic acid synthesis. The aspartate nitrogen can be used for synthesis of pyrimidines (green path) or urea (blue path). In ASS1 deficiency (CTLN I) there is a potential diversion of the aspartate towards pyrimidine whereas in citrin deficiency (CTLN II) aspartate is not transported across the mitochondria. ASA, argininosuccinate; ARG, arginase. **b**, Prediction by the generic human model; decreasing ASS1 activation (green line) results in an increase in the cellular growth rate and in the flux through the CAD reaction (blue line); a.u., arbitrary units. **c**, Urinary orotic acid levels are elevated significantly in patients with CTLN I compared with normative values in control subjects (0.3–2.8 mmol mol^{-1} creatinine, depicted by the red dashed line), and with those with CTLN II. $^{**}P < 0.005$ using log-transformed data for *t*-test analysis ($n = 5$ with CTLN I and $n = 4$ with CTLN II). **d–g**, These experiments were repeated twice with pooled cells from two patients with CTLN II, from one patient with CTLN I and from three control subjects. Statistical analysis used one-way analysis of variance (ANOVA). Error bars represent standard error. **d**, Significantly lower levels of pyrimidines in CTLN II fibroblasts compared with CTLN I and with normal fibroblasts. TMP was undetectable. **e**, Top: crystal violet staining on day 5 shows increased proliferation in CTLN I compared with CTLN II and with normal control. Bottom: a quantification graph for the staining. (ANOVA; $^{***}P < 0.0005$). **f**, **g**, Primary fibroblasts from CTLN I subjects have increased levels of aspartate (**f**) and uracil (**g**) compared with fibroblasts from patients with CTLN II and with normal controls (ANOVA, Tukey's honest significant difference test, $^{*}P < 0.0005$). This is a representative graph of three independent experiments. **h**, Left: a small-intestine tissue section of a mouse was hybridized with FISH probe libraries for single *Ass1* (green dots) and for *Ki67* mRNA molecules (red dots). Nuclei were stained with DAPI (4′,6-diamidino-2-phenylindole; blue). Dashed line outlines the crypt bottom. White lines mark cell borders according to co-immunofluorescence staining with FITC-E-cadherin. A magnifying window highlights a clear demarcation of *Ass1* mRNA localizing to the differentiated cells of the crypt (magnification ×100). Goblet cells exhibit some non-specific fluorescence appearing in multiple channels. Right: quantified correlations between *Ass1* and *Glut2*, an enterocyte marker (top), and between *Ass1* and *Ki67* (bottom).

their 'routine pathways' for the synthesis of biological molecules that are essential for cell division and growth. We hence conducted an analysis of *ASS1* expression data in cancer cell lines from the NCI-60 collection and found a significant inverse correlation between *ASS1* expression levels and the reported doubling time of the cancerous cells (Fig. 2a). To further test whether this correlation is explicable by diversion of aspartate flux, we used our modelling program and predicted that, with *ASS1* inactivation, there is an accompanying significant increase in aspartate flux through the relevant metabolic reactions for nucleic acid synthesis (Extended Data Table 1). In contrast, modelling the inactivation of ASL predicted an endogenous arginine depletion that does not directly affect the flux towards nucleic-acid synthesis (data not shown). Furthermore, analysis of The Cancer Genome Atlas database for *ASL* and *ASS1* expression shows that these genes can both be downregulated in the same cancers, suggesting that they are not mutually exclusive (Extended Data Fig. 1d). Thus, *ASS1* silencing in cancerous proliferation might have an arginine-independent effect that is related to nucleotide synthesis.

Using specific metabolic models tailored for each of the NCI-60 cell lines[10], we further predicted that 8 out of the 13 metabolites computationally shown to be increased with *ASS1* inactivation were nucleic acids (Fig. 2b and Extended Data Fig. 1e). Additionally, specific analysis of the TCGA database of tumours where *ASS1* expression is downregulated showed a significant upregulation in the expression of *CAD*, compared with the paired normal tissue (Fig. 2c). We further confirmed the inverse upregulation in the expression of *CAD* versus *ASS1* at the mRNA level in the NCI-60 cancer cell-line database as well as in independent databases for patients with osteosarcoma[11] and melanoma[12]; we found that downregulation of *ASS1* and upregulation of *CAD* are in concordance with cancerous phenotype (Extended Data Fig. 1f, g). In addition, we demonstrated the inverse expression levels between ASS1 and CAD at the protein level using osteosarcoma and melanoma cell lines that differ in their expression pattern of ASS1 (Extended Data Figs 1h and 2a). To validate these modelling and global informatics analyses with experimental evidence, we studied osteosarcoma cell lines in which ASS1 was either deficient (MNNG/HOS) or present (U2OS) (Fig. 2d and Supplementary Fig. 1). Metabolic analyses confirmed that cells deficient in ASS1 had an increase in pyrimidine levels, an increase in the level of uracil as well as a significantly increased proliferation rate (Fig. 2e–g) compared with osteosarcoma cells having higher levels of ASS1. We additionally verified these results in melanoma cell lines that differed in their level of ASS1 expression (Extended Data Fig. 2b–d).

To definitively demonstrate the direct correlation between ASS1 expression and proliferation and to differentiate it from other metabolic

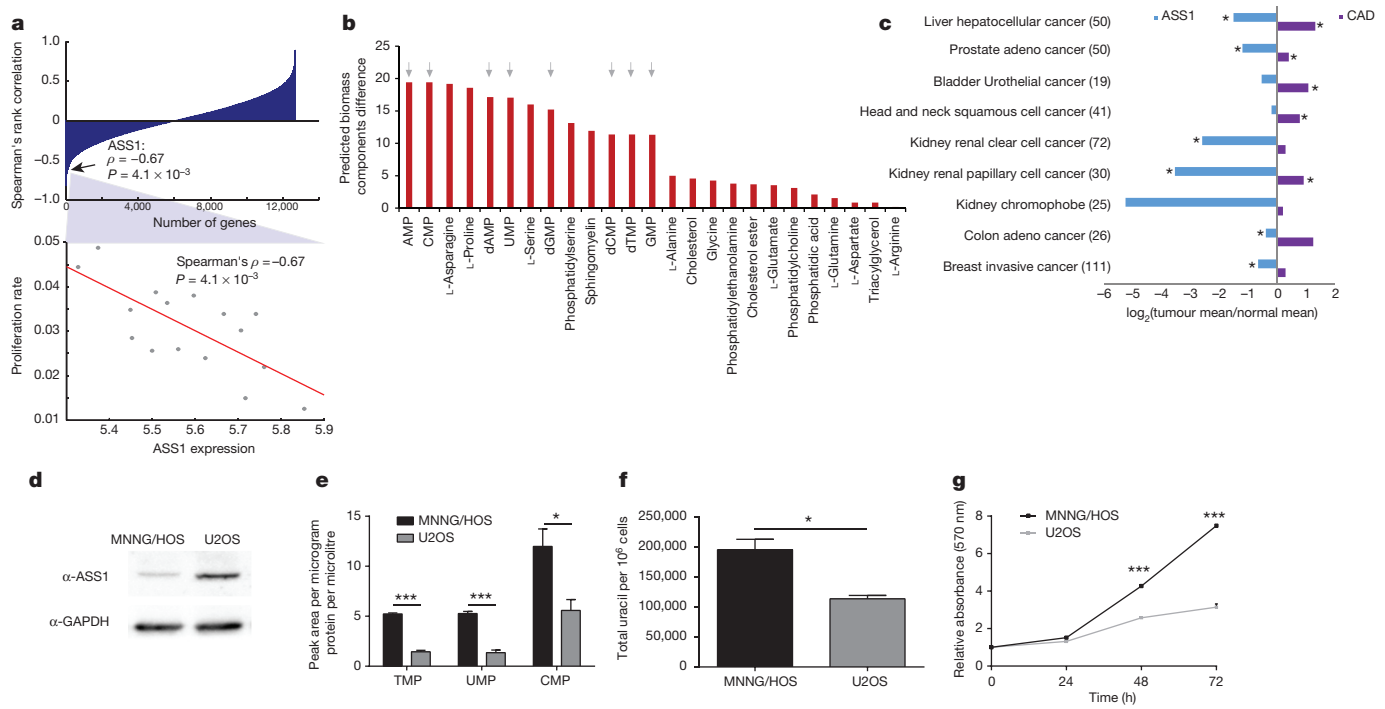

Figure 2 | ASS1-deficient tumours have increased proliferation rate and pyrimidine levels. a, Top: *ASS1* is ranked within the top 24 genes out of 14,000, that show a significant inverse correlation with proliferation rate among the 16 NCI-60 cancer cell lines in which ASS1 is downregulated; Spearman's rank correlation was calculated between the expression of each gene and its associated proliferation rates. Bottom: magnified view of the correlation between proliferation rate and *ASS1* expression levels. **b**, Predicted differences in the production rate of biomass components after the inactivation of *ASS1*. The production of nucleic acids marked in arrows, is predicted to have a large increase after *ASS1* inactivation in most of the NCI-60 cell lines. The figure represents the results obtained using the LOX IMVI cell line model; however, the same results were seen for all NCI-60 cell lines as well as in using the human generic model. The models used are based on a series of simplifying assumptions as described by us previously in detail[10]. **c**, Analysis of the TCGA database of matched tumour–normal tissue pairs showing that *CAD* expression is elevated significantly in tumours with *ASS1* downregulation compared with normal tissue ($*P < 0.05$). **d**, Immunoblot of osteosarcoma cell lines showing decreased expression of ASS1 compared with the loading control GAPDH in MNNG/HOS compared with U2OS. **e**, Osteosarcoma cells with ASS1 downregulation have a significant increase in pyrimidine levels as measured by LC–MS ($n \geq 3$; $*P < 0.05$; $***P < 0.0005$). Error bars are standard error. **f**, Osteosarcoma cells with ASS1 downregulation have a significant increase in uracil ($n = 3$; $*P < 0.05$). Error bars are standard error. **g**, Osteosarcoma cells with ASS1 downregulation have a significant increase in proliferation as measured by MTT assay ($***P < 0.0005$).

changes that occur in cancer cells, we overexpressed ASS1 in MNNG/HOS, and knocked it down in U2OS cells (Fig. 3a). Our results clearly show that changes in ASS1 levels inversely alter the proliferation rate and pyrimidine synthesis in these cells (Fig. 3b–e and Extended Data Fig. 3a–f). If the major determinant by which ASS1 overexpression decreases proliferation is through diverting aspartate metabolism away from pyrimidine synthesis, supplementation with nucleic acids should restore proliferation. Indeed, supplementing the media with nucleic acids, specifically with pyrimidines, significantly restores the proliferation of ASS1-overexpressing cells to a similar level as the parental cell line (Fig. 3f and Extended Data Fig. 2e–j). Thus, in two distinct forms of cancer, changes in ASS1 expression levels directly affect aspartate utilization for pyrimidine synthesis and proliferation. Importantly, similar results were obtained *in vivo*; mice injected with melanoma cells knocked down for *ASS1* developed tumours that grew more rapidly and had higher levels of total and M + 1-labelled aspartate and uracil than the parental tumour cells that expressed the empty vector (Fig. 3g, h and Extended Data Fig. 3g).

An expected synergistic way to increase aspartate delivery for pyrimidine synthesis would be by upregulation of citrin. Analysis of the TCGA database showed that in tissues that normally do not express citrin (also known as SLC25A13) at high levels[13], there is a significantly elevated expression in the cancerous state (Extended Data Fig. 4b). In addition, in the liver where citrin is strongly expressed, a recent publication of ASS1 expression in hepatocellular carcinoma showed that downregulation of ASS1 is associated with a more malignant cancerous phenotype[14]. These results, together with our study of primary human fibroblast cells (Fig. 1c–g), imply that proliferation induced by loss of ASS1 in tumours might be counteracted by inhibiting citrin. Indeed, *si-citrin* in U2OS decreases proliferation significantly when ASS1 levels are reduced (Fig. 4a). Use of *si-citrin* also decreases pyrimidine levels as well as total and labelled levels of M + 1 aspartate and of M + 1 orotic acid (Fig. 4b, c and Extended Data Fig. 4c, d). As citrin is part of the malate–aspartate shuttle, its deficiency is expected to affect several aspects in cell survival and growth. Our results indicate that citrin function in transferring mitochondrial-derived aspartate is important for supplying substrate for pyrimidine synthesis, especially in cancers with ASS1 downregulation. These findings are therapeutically relevant as survival analysis of several cancers in the TCGA database reveals that cancers with decreased *ASS1* expression and high *citrin* levels have a trend for significantly worse prognosis (Fig. 4d, Extended Data Fig. 4e and Extended Data Table 2).

The use of citrin-derived aspartate by CAD requires CAD activation. Recently, CAD was shown to be activated by ribosomal protein S6 kinase (S6K1), regulated by the mTOR pathway[15]. When ASS1 expression in cancer cells is decreased, we find increased phosphorylation of S6K1 and CAD that is reduced by *si-citrin*, implying that aspartate levels are important in regulating the mTOR pathway activation (Fig. 4e and Extended Data Fig. 4f). In addition, we show a significant increase in the location proximity between CAD and citrin after ASS1 downregulation (Extended Data Fig. 4g). Thus, aspartate regulates pyrimidine levels by regulating CAD's substrate availability, protein localization and activity. Consistent with this, we see a decrease in proliferation when ASS1-deficient cells are treated either with the mTOR inhibitor rapamycin or with thymidylate synthase inhibitor 5-fluorouracil (5FU) (Fig. 4f). Importantly, rapamycin treatment is accompanied by a

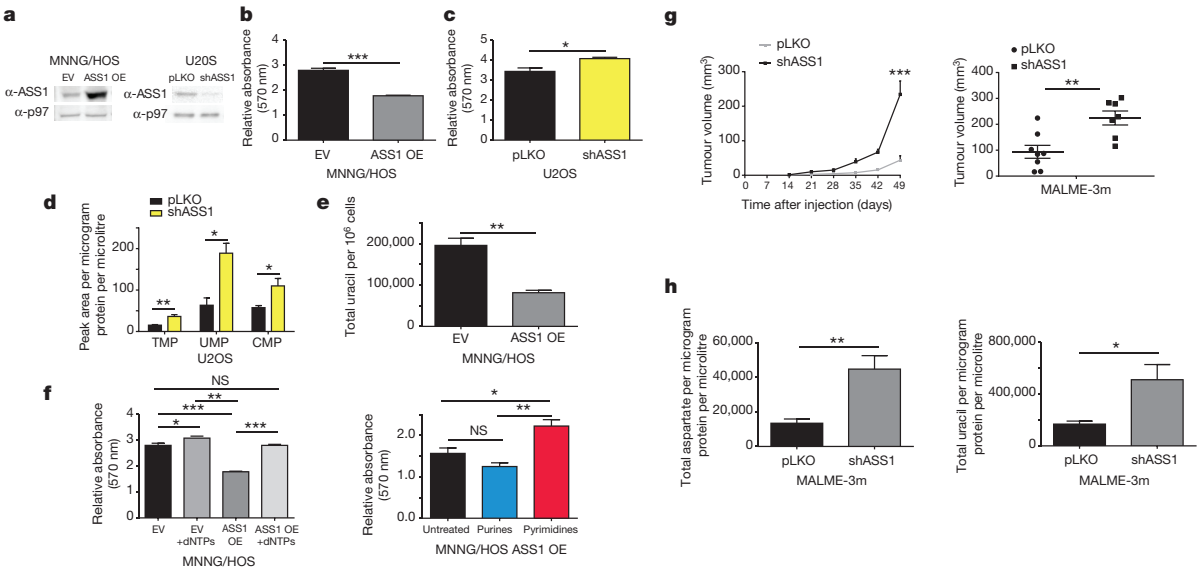

Figure 3 | ASS1 expression levels in cancer determine aspartate availability for pyrimidine synthesis. a, Immunoblots of osteosarcoma cells after transduction with either *ASS1* overexpression construct (left) or with *ASS1-shRNA* (right). **b**, MTT proliferation assay in osteosarcoma cells showing a significant decrease in proliferation after ASS1 overexpression (***$P < 0.0005$). **c**, MTT proliferation assay in osteosarcoma cells showing a significant increase in proliferation after transduction with *shASS1* (*$P < 0.05$). The proliferation values are shown for day 3, after normalizing the data for the reading after cell adherence ($n \geq 3$). **d**, LC–MS measurements of pyrimidine levels showing a significant increase after the use of *ASS1-shRNA* in osteosarcoma cells ($n \geq 3$). **e**, Total uracil is decreased significantly in osteosarcoma cells with ASS1 overexpression ($n \geq 3$; **$P = 0.005$). **f**, Left: dNTP supplementation rescues proliferation after ASS1 overexpression in osteosarcoma cells. Right: pyrimidines significantly rescue proliferation in ASS1-overexpressing MNNG/HOS cells ($n \geq 3$; *$P < 0.05$, **$P < 0.005$, ***$P < 0.0005$). **g**, **h**, Ten million MALME-3m melanoma cells transduced with either pLKO empty vector or with *shASS1* were injected subcutaneously to immune-deficient mice. The experiment was repeated three times. After euthanasia, the tumours were removed, measured and incubated with labelled [^{15}N]α-glutamine for 6 h. Two weeks after injection, the group injected with melanoma cells with *shASS1* developed tumours that grew more rapidly in size (**g**, left) and were hence significantly larger when removed (**g**, right). The experiment was repeated three times with similar results (**$P < 0.005$, ***$P < 0.0005$). **h**, Tumours with shASS1 had higher levels of total aspartate (left) and total uracil (right) than those expressing the empty vector. Statistical analysis used repeated-measurements ANOVA ($n = 15$; *$P < 0.05$; **$P < 0.005$). All error bars are standard error.

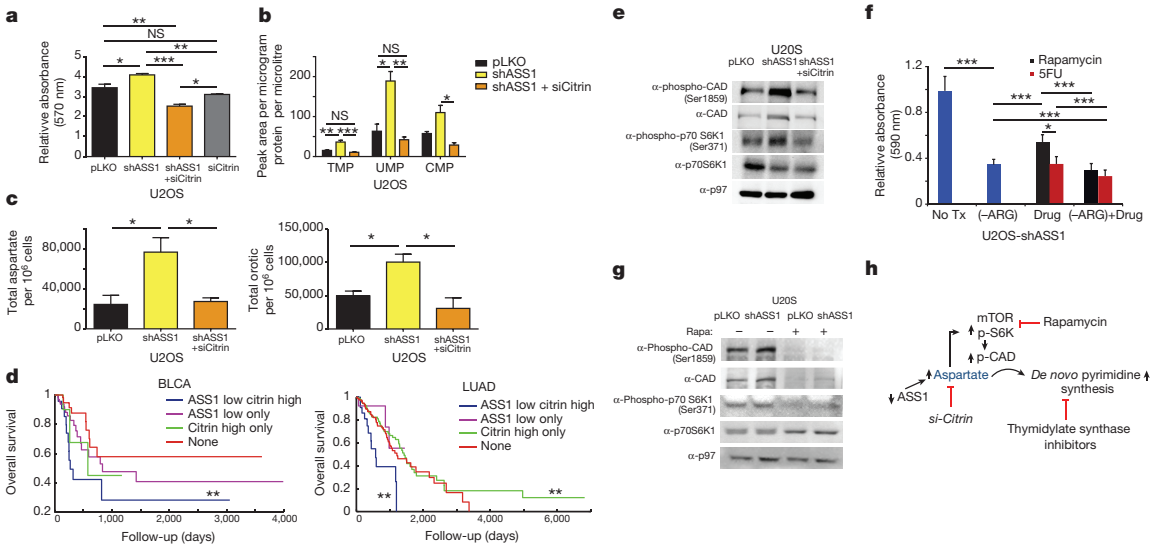

Figure 4 | Decreasing CAD activation reduces proliferation in ASS1-deficient cancers. a, MTT assay showing that decreasing citrin levels significantly decreases proliferation in U2OS osteosarcoma, even after a significant proliferation increase is accomplished by ASS1 downregulation ($n \geq 3$; *$P < 0.05$; **$P < 0.005$; ***$P < 0.0005$). **b**, Decreasing citrin levels decreases pyrimidine levels in U2OS cells with ASS1 downregulation ($n \geq 3$; *$P < 0.05$). **c**, GC–MS measurements showing that U2OS with *shASS1* has a significant increase in total aspartate (left), as well as in total orotic acid (right), which are reversed when transfected with *si-citrin* ($n \geq 3$; ANOVA, Tukey's honest significant difference test, *$P < 0.05$). Error bars are standard error. **d**, Kaplan–Meier survival analysis for two different cancer types (BLCA, bladder cancer; LUAD, lung adenocarcinoma), both showing significantly poor survival for cancers with low ASS1 and high citrin expression levels ($n \geq 3$; **log rank $P \leq 0.005$). **e**, Immunoblot of osteosarcoma cells for the mTOR pathway downstream effectors S6K1 and CAD showing increased phosphorylation after *shASS1* that is reversed when cells are transfected with si-citrin. **f**, Quantification graph of crystal violet staining of osteosarcoma cells transduced with shASS1 after drug treatments (Tukey's post-hoc; $P < 0.0005$). All treatments were significant compared with no treatment. In addition, the results show a significant beneficial effect of decreased proliferation in response to treatment with either mTOR or pyrimidine synthesis inhibitors (rapamycin or 5FU respectively), with 5FU being more beneficial than rapamycin ($P < 0.0005$). Of note, 5FU had a significant additive beneficial effect when added as treatment to arginine-deleted medium (Tukey's post-hoc test; $P < 0.0005$). Cells were grown in normal medium, in medium depleted of arginine, in complete medium with either rapamycin or 5FU, and in arginine-depleted medium together with either rapamycin or 5FU ($n = 9$; ***$P < 0.0005$). **g**, Western blot showing decreased activation of the mTOR proteins after rapamycin treatment. **h**, Schematic presentation for potential interventions in pyrimidine synthesis in ASS1-deficient tumours.

decrease in CAD phosphorylation (Fig. 4g). Hence, targeting aspartate transport could be an additional therapeutic option in cancers with ASS1 silencing, especially in those that develop resistance to arginine-depleting agents (Fig. 4h).

In summary, our studies demonstrate that ASS1, a urea cycle enzyme, facilitates pyrimidine synthesis in cancerous proliferation by activating CAD, through regulation of aspartate levels. There are several clinical trials in patients with ASS1-deficient hepatocellular carcinoma and mesothelioma, which combine arginine-depleting agents with thymidylate synthase inhibitors such as capecitabine and pemetrexed (http://clinicaltrials.gov, NCT02089633, NCT02029690). We believe our study provides the rationale for such therapeutic modalities and hence has direct translational relevance.

Online Content Methods, along with any additional Extended Data display items and Source Data, are available in the online version of the paper; references unique to these sections appear only in the online paper.

Received 17 November 2014; accepted 27 August 2015.
Published online 11 November 2015.

1. Dimmock, D. *et al.* Citrin deficiency, a perplexing global disorder. *Mol. Genet. Metab.* **96,** 44–49 (2009).
2. Delage, B. *et al.* Arginine deprivation and argininosuccinate synthetase expression in the treatment of cancer. *Int. J. Cancer* **126,** 2762–2772 (2010).
3. Long, Y. *et al.* Arginine deiminase resistance in melanoma cells is associated with metabolic reprogramming, glucose dependence, and glutamine addiction. *Mol. Cancer Ther.* **12,** 2581–2590 (2013).
4. Morris, S. M., Jr. Recent advances in arginine metabolism: roles and regulation of the arginases. *Br. J. Pharmacol.* **157,** 922–930 (2009).
5. Wheatley, D. N. Controlling cancer by restricting arginine availability–arginine-catabolizing enzymes as anticancer agents. *Anticancer Drugs* **15,** 825–833 (2004).
6. Syed, N. *et al.* Epigenetic status of argininosuccinate synthetase and argininosuccinate lyase modulates autophagy and cell death in glioblastoma. *Cell Death Dis.* **4,** e458 (2013).
7. Duarte, N. C. *et al.* Global reconstruction of the human metabolic network based on genomic and bibliomic data. *Proc. Natl Acad. Sci. USA* **104,** 1777–1782 (2007).
8. Kobayashi, K., Saheki, T. & Song, Y. Z. Citrin deficiency. *GeneReviews* http://www.ncbi.nlm.nih.gov/books/NBK1181/ (2005).
9. Marion, V. *et al.* Hepatic adaptation compensates inactivation of intestinal arginine biosynthesis in suckling mice. *PLoS One* **8,** e67021 (2013).
10. Yizhak, K. *et al.* Phenotype-based cell-specific metabolic modeling reveals metabolic liabilities of cancer. *eLife* **3,** e03641 (2014).
11. Kuijjer, M. L. *et al.* IR/IGF1R signaling as potential target for treatment of high-grade osteosarcoma. *BMC Cancer* **13,** 245 (2013).
12. Kabbarah, O. *et al.* Integrative genome comparison of primary and metastatic melanomas. *PLoS One* **5,** e10770 (2010).
13. del Arco, A. *et al.* Expression of the aspartate/glutamate mitochondrial carriers aralar1 and citrin during development and in adult rat tissues. *Eur. J. Biochem.* **269,** 3313–3320 (2002).
14. Tan, G. S. *et al.* Novel proteomic biomarker panel for prediction of aggressive metastatic hepatocellular carcinoma relapse in surgically resectable patients. *J. Proteome Res.* **13,** 4833–4846 (2014).
15. Ben-Sahra, I., Howell, J. J., Asara, J. M. & Manning, B. D. Stimulation of de novo pyrimidine synthesis by growth signaling through mTOR and S6K1. *Science* **339,** 1323–1328 (2013).

Supplementary Information is available in the online version of the paper.

Acknowledgements We thank A. Gross and B. Lee for discussions. We acknowledge and thank the Weizmann Institute for providing financial and infrastructural support and the Baylor College of Medicine Biochemical Laboratory. We appreciate the statistical analysis by R. Rotkopf and the technical contributions of A. Tishbee, T. Kaufman, D. Laufer and I. Rogachev. A.E. is the incumbent of the Leah Omenn Career Development Chair and is supported by research grants from the European Research Program (CIG618113, ERC614204), the Israel Science Foundation (1343/13; 1952/13) and a Minerva grant award (711730). A.E. received additional support from the Adelis Foundation, the Henry S. and Anne S. Reich Research Fund, the Dukler Fund for Cancer Research, the Paul Sparr Foundation, the Saul and Theresa Esman Foundation, from Joseph Piko Baruch and from the estate of Fannie Sherr. L.A. was supported by a postdoctoral fellowship from Teva. The research of K.Y. and E.R. has been supported by grants from the Israeli Science Foundation (E.R.), the Israeli Cancer Research Fund (E.R.), the Israeli Center of Excellence (I-CORE) Program of the Planning and Budgeting Committee and Israel Science Foundation Grant No. 41/11 (E.R.). A.Sa. is supported by the Israel Cancer Research Foundation and S.N.S.C. is supported by a Baylor College of Medicine Intellectual and Developmental Disabilities Research Center Grant (number 1 U54 HD083092) from the Eunice Kennedy Shriver National Institute of Child Health & Human Development, and by the Doris Duke Charitable Foundation (DDCF 2013095). I.U. was supported by a grant from the Rising Tide Foundation and by a research grant from The Abramson Family Center for Young Scientists.

Author Contributions S.R. performed most of the experiments described in the manuscript; L.A. set up the system that allowed us to test our hypothesis; K.Y and E.R designed the modelling analysis. K.Y. from the laboratory of E.R. performed the modelling analysis; A.Sa. performed *in vitro* studies with the patients' cells and helped establish the *in vivo* models; A.Si. executed the metabolic analysis by gas chromatography–mass spectrometry (GC–MS); S.A. helped with the *si-citrin* experiments; N.S. performed the *in vivo* experiments; Q.S. analysed levels of orotic acid in the patients' urine; A.B. performed the pyrimidine analysis by liquid chromatography–mass spectrometry (LC–MS); D.H., S.K. and D.D. provided data and primary cell lines from patients with CTLN II; S.I. and S.A. performed the fluorescence *in situ* hybridization (FISH) experiments of the mouse intestine; I.U. analysed the TCGA database; S.C.S.N. provided primary cells of patients with CTLN I as well as help writing the manuscript; A.E. was the leading principal investigator who initiated and directed the study and co-wrote the paper with inputs from all authors. K.Y., A.Si., S.H. and A.Sa. contributed equally to this work.

Author Information Reprints and permissions information is available at www.nature.com/reprints. The authors declare no competing financial interests. Readers are welcome to comment on the online version of the paper. Correspondence and requests for materials should be addressed to A.E. (ayelet.erez@weizmann.ac.il).

METHODS

Unless mentioned otherwise, the experiments were not randomized and the investigators were not blinded to allocation during experiments and outcome assessment.

Measurements in human subjects. The fibroblast studies were performed on anonymized cells devoid of all identifiers. The data analysis involving urine orotic acid levels were performed under a protocol approved by the Institutional Review Board of Baylor College of Medicine. Urine samples were prepared by mixing 200 µl of with isotopic internal standard [$^{15}N_2$]orotic acid (Cambridge Isotope Laboratories). Orotic acid and orotidine were assayed on a Micromass Quattro mass spectrometer (Waters). HPLC was performed on a Waters ODS-AQ analytical column (150 mm × 2.0 mm internal diameter 5 µm bead size). Mobile phase was isocratic 0.05 M ammonium formate (pH 4.0). The MS–MS system was set at a flow rate of 0.2 ml min^{-1}. The mass spectrometer was operated in electrospray ionization negative multiple-reaction monitoring mode. Nitrogen was used as nebulizer gas at a flow rate of 60–90 l h^{-1} and desolvation gas 500 l h^{-1}. Other optimized mass spectrometer parameters were cone voltage 15 V, capillary 3,250 V and collision voltage 10 V.

Genome-scale metabolic modelling. A metabolic network consisting of m metabolites and n reactions can be represented by a stoichiometric matrix S, where the entry S_{ij} represents the stoichiometric coefficient of metabolite i in reaction j[17]. A constraint-based mode imposes mass balance, directionality and flux capacity constraints on the space of possible fluxes in the metabolic network's reactions through a set of linear equations:

$$^{i}S \times v = 0 \quad (1)$$

$$v_{\min} \leq v \leq v_{\max} \quad (2)$$

where v stands for the flux vector for all of the reactions in the model (that is, the flux distribution). The exchange of metabolites with the environment is represented as a set of exchange (transport) reactions, enabling a pre-defined set of metabolites to be either taken up or secreted from the growth media. The steady-state assumption represented in equation (1) constrains the production rate of each metabolite to be equal to its consumption rate. Enzymatic directionality and flux capacity constraints define lower and upper bounds on the fluxes and are embedded in equation (2). In the following, flux vectors satisfying these conditions will be referred to as feasible steady-state flux distributions. The analyses were performed under the Roswell Park Memorial Institute Medium (RPMI)-1640m. We used the biomass function introduced in ref. 16.

Predicting growth rate, metabolite production and flux distribution through metabolic modelling. To determine the relation between ASS1 activity, CAD activity and growth rate, we used a generic human model and simulated the inactivation and activation of the reaction catalysed by ASS1. The inactivation was simulated by constraining the flux through the ASS1 reaction to zero, while the activation was simulated by enforcing increased positive flux through the ASS1 reaction up to the maximal possible flux, as computed via flux variability analysis[17]. At each such point, the maximal growth rate was computed via flux balance analysis[17]. Additionally, we estimated the flux through the reaction catalysed by CAD under maximal growth rate on the basis of 1,000 different feasible flux samples[18].

We next used genome-scale metabolic models for each of the NCI-60 cancer cell lines on the basis of their gene expression measurements[10]. In each cell-line model, we performed the following analyses. (1) We computed the production of each biomass component under both the inactivation and maximal activation of ASS1, as described above. The difference between the predicted production rates of each biomass component in the two states was then computed on the basis of the results of this optimization problem. (2) Similarly, we examined the flux change of each reaction under maximal biomass production in both the inactivation and activation states, as described above. In each of these states, we sampled the solution space and obtained 1,000 feasible flux distributions[18]. Focusing on the reactions associated with aspartate and glutamine, we computed the fold-change in flux rate together with its significance level. The latter was computed via a two-sided Wilcoxon rank-sum test. The largest fold-change among these reactions was predicted for the reactions catalysed by the CAD enzyme.

TCGA data analysis. For each tumour, normalized gene expression levels measured using RSEM[19] were obtained from the RNASeqV2 data sets at the TCGA portal (https://tcga-data.nci.nih.gov/tcga/). Only matched tumour–normal pairs were used. For each tumour type, we computed the mean expression levels in the tumour and normal samples, added a pseudo-count of 1 to each mean and plotted the ratio between the means.

Metabolomics analysis. Osteosarcoma or melanoma cell lines were seeded at 3×10^6 to 5×10^6 cells per 10 cm plate and incubated with either 4 mM L-glutamine, (α-^{15}N, 98%, Cambridge Isotope Laboratories) for 24 h. Subsequently, cells were washed with ice-cold saline, lysed with 50% methanol in water and quickly scraped followed by three freeze–thaw cycles in liquid nitrogen. The insoluble material was pelleted in a cooled centrifuge (4 °C) and the supernatant was collected for consequent GC–MS analysis. Samples were dried under air flow at 42 °C using a Techne Dry-Block Heater with sample concentrator (Bibby Scientific) and the dried samples were treated with 40 µl of a methoxyamine hydrochloride solution (20 mg ml^{-1} in pyridine) at 37 °C for 90 min while shaking followed by incubation with 70 µl *N*,*O*-bis (trimethylsilyl) trifluoroacetamide (Sigma) at 37 °C for an additional 30 min.

GC–MS. GC–MS analysis used a gas chromatograph (7820AN, Agilent Technologies) interfaced with a mass spectrometer (5975 Agilent Technologies). An HP-5ms capillary column 30 m × 250 µm × 0.25 µm (19091S-433, Agilent Technologies) was used. Helium carrier gas was maintained at a constant flow rate of 1.0 ml min^{-1}. The GC column temperature was programmed from 70 to 150 °C via a ramp of 4 °C min^{-1}, 250–215 °C via a ramp of 9 °C min^{-1}, 215–300 °C via a ramp of 25 °C min^{-1} and maintained at 300 °C for an additional 5 min. The MS was by electron impact ionization and operated in full-scan mode from m/z = 30–500. The inlet and MS transfer line temperatures were maintained at 280 °C, and the ion source temperature was 250 °C. Sample injection (1 µl) was in splitless mode.

Nucleic acid analysis. *Materials.* Ammonium acetate (Fisher Scientific) and ammonium bicarbonate (Fluka) of LC–MS grade were used. Sodium salts of AMP, CMP, GMP, TMP and UMP were obtained from Sigma-Aldrich. Acetonitrile of LC grade was supplied from Merck. Water with resistivity 18.2 MΩ was obtained using Direct 3-Q UV system (Millipore).

Extract preparation. The obtained samples were concentrated in speedvac to eliminate methanol, and then lyophilized tol dryness, re-suspended in 200 µl of water and purified on polymeric weak anion columns (Strata-XL-AW 100 µm (30 mg ml^{-1}, Phenomenex)) as follows. Each column was conditioned by passing 1 ml of methanol, then 1 ml of formic acid/methanol/water (2/25/73) and equilibrated with 1 ml of water. The samples were loaded, and each column was washed with 1 ml of water and 1 ml of 50% methanol. The purified samples were eluted with 1 ml of ammonia/methanol/water (2/25/73) followed by 1 ml of ammonia/methanol/water (2/50/50) and then collected, concentrated in speedvac to remove methanol and lyophilized. Before LC–MC analysis, the obtained residues were re-dissolved in 100 µl of water and centrifuged for 5 min at 21,000 *g* to remove insoluble material.

LC–MS analysis. The LC–MS/MS instrument consisted of an Acuity I-class UPLC system (Waters) and Xevo TQ-S triple quadruple mass spectrometer (Waters) equipped with an electrospray ion source and operated in positive ion mode was used for analysis of nucleoside monophosphates. MassLynx and TargetLynx software (version 4.1, Waters) were applied for the acquisition and analysis of data. Chromatographic separation was done on a 100 mm × 2.1 mm internal diameter, 1.8-µm UPLC HSS T3 column equipped with 50 mm × 2.1 mm internal diameter, 1.8-µm UPLC HSS T3 pre-column (both Waters Acuity) with mobile phases A (10 mM ammonium acetate and 5 mM ammonium hydrocarbonate buffer, pH 7.0 adjusted with 10% acetic acid) and B (acetonitrile) at a flow rate of 0.3 ml min^{-1} and column temperature 35 °C. A gradient was used as follows: for 0–6 min the column was held at 0% B, then 6–6.5 min a linear increase to 100% B, 6.5–7.0 min held at 100% B, 7.0–7.5 min back to 0% B and equilibration at 0% B for 2.5 min. Samples kept at 8 °C were automatically injected in a volume of 3 µl.

For mass spectrometry, argon was used as the collision gas with a flow of 0.25 ml min^{-1}. The capillary voltage was set to 2.90 kV, source temperature 150 °C, desolvation temperature 350 °C, desolvation gas flow 650 l min^{-1}. Analytics were detected using multiple-reaction monitoring and applying the parameters listed in Supplementary Table 3.

Hybridizations and imaging. Single-molecule FISH (smFISH) was performed with probe libraries for Ass1 (74 probes, sequences described in Supplementary Methods) and Ki67 (96 probes[20]). Imaging was performed as previously described[20]. smFISH images were filtered with a Laplacian of Gaussian filter of size 15 pixels and standard deviation of 1.5 pixels. Each image is a maximum projection of ten stacks spaced 0.3 µm apart in the z-direction. Each dot in these figures represents a cell and the quantification dots were counted on eight z-stacks spaced 0.3 µm apart (total tissue volume 2.4 µm).

Proximity ligation assay. The assay was performed as published[21] using Sigma Aldrich kit (DUO 92004-30-RXN). Antibodies used for detection were diluted in PBS: ASS1 (1:200, ab170952, abcam), citrin (1:100, H00010165-M01, clone 4F4, abnova) and anti-CAD (1:100, ab40800, abcam).

Cell cultures. All cell lines were authenticated. Melanoma cell lines LOX IMVI and MALME-3m and osteosarcoma cell lines MNNG/HOS and U2OS were purchased from American Type Culture Collection (ATCC) and cultured using standard

procedures in a 37 °C humidified incubator with 5% CO_2 in RPMI (Invitrogen) supplemented with 10–20% heat-inactivated fetal bovine serum, 10% pen-strep and 2 mM glutamine. All cells are tested routinely for mycoplasma using a Mycoplasma EZ-PCR test kit (20–700-20, Biological Industries).

Proliferation assays. *MTT assay*. Cells were seeded in 12-well plates at 4×10^4 to 8×10^4 cells per well in a triplicate. After 6 h for adherence of the cells, 0.1 mg ml^{-1} of MTT (3-(4,5-dimethylthiazol-2-yl)-2,5 diphenyltetrazolium bromide) (CAS 298-93-1, Calbiochem) in PBS was added to each cell type, starting at 0 h, in 24 h intervals. Deoxynucleotide Set (DNTP100-1KT, Sigma-Aldrich) was added to the cells' medium first after adherence and then daily at a final concentration of 10 μM. Cells were lysed with dimethylsulfoxide (DMSO). Absorbance was measured at 570 nm.

Crystal violet staining. Cells were seeded in 12-well plates at 40,000–100,000 cells per well in a triplicate. Time 0 was calculated as the time the cells became adherent, which was after about 6 h from plating. For each time point, cells were washed with PBS X1 and fixed in 4% PFA (in PBS). Cells were then stained with 0.1% Crystal Violet (C0775, Sigma-Aldrich) for 20 min (1 ml per well) and washed with water. Cells were then incubated with 10% acetic acid for 20 min with shaking. Extract was then diluted 1:4 in water and absorbance was measured at 590 nm every 24 h.

Protein and RNA analysis. *Western blotting*. Cells were lysed in RIPA (Sigma-Aldrich) and 0.5% protease inhibitor cocktail (Calbiochem). After centrifugation, the supernatant was collected and protein content was evaluated by the Bradford assay. One hundred micrograms from each sample under reducing conditions were loaded into each lane and separated by electrophoresis on a 10% SDS polyacrylamide gel. After electrophoresis, proteins were transferred to Immobilon transfer membranes (Tamar). Non-specific binding was blocked by incubation with TBST (10 mM Tris–HCl (pH 8.0), 150 mM NaCl, 0.1% Tween 20) containing 3% albumin from bovine serum for 1 h at 25 °C. Membranes were subsequently incubated with antibodies against ASS1 (1:500, sc-99178, Santa Cruz Biotechnology)[22], p97 (1:10,000, PA5-22257, Thermo Scientific), GAPDH (1:1,000, 14C10, 2118, Cell Signaling)[23], CAD (1:1,000, ab40800, abcam)[24], phospho-CAD (Ser1859) (1:1,000, 12662, Cell Signaling)[15], p70 S6 Kinase (1:1,000, 9202, Cell Signaling) and phospho-p70 S6 Kinase (Ser371) (1:1,000, 9208, Cell Signaling)[25]. Antibody was detected using peroxidase-conjugated AffiniPure goat anti-rabbit IgG or goat anti-mouse IgG (Jackson ImmunoResearch) and enhanced chemiluminescence western blotting detection reagents (EZ-Gel, Biological Industries).

Gels were quantified by Gel Doc XR+ (BioRad) and analysed by ImageLab 4.1 software (BioRad). The band area was calculated by the intensity of the band. The obtained value was then divided by the value obtained from the loading control.

RNA extraction and complementary DNA (cDNA) synthesis. RNA was extracted from cells by using PerfectPure RNA Cultured Cell Kit (5′-PRIME). cDNA was synthesized from 1 μg RNA by using qScript cDNA Synthesis Kit (Quanta).

Quantitative PCR. Detection of *ASS1* on cDNAs (see above) was performed using SYBR green PCR master mix (Tamar) and the required primers. Primer sequences were as follows. Human *ASS1*: forward, 5′-TTATAACCTGGGATGGGCACC-3′; reverse, 5′-TGGACATAGCGTCTGGGATTG-3′. Human *HPRT*: forward, 5′-ATTGACACTGGCAAAACAATGC-3′; reverse,: 5′-TCCAACACTTCG TGGGGTCC-3′. Analysis used StepOne real-time PCR technology (Applied Biosystems).

Transient transfection. Cells were seeded in 12-well plates at 30,000 cells per well, or in 10 cm plates at 10^6 cells per plate, in triplicate. The following day, cells were transfected with either 20 pmol or 600 pmol siRNA siGenome SMARTpool targeted to Citrin mRNA (M-007472-01, Thermo Scientific), respectively. Transfection was performed with Lipofectamine 2000 Reagent (11668-019, Invitrogen) in the presence of Opti-MEM I Reduced Serum Medium (31985-062, Invitrogen). Four hours after transfection, medium was replaced and experiments were performed starting 24 h after transfection.

Infection. Over-expression. Cells were infected with pLenti3.3/TR and with pLenti6.3/TO/V5-DEST-based lentiviral vector with or without the human ASS1 transcript. Transduced cells were selected with 1 mg ml^{-1} Geneticin and with 7.5 μg ml^{-1} Blasticidin for each plasmid, respectively. When induction of expression was needed, cells were added with 10 μg ml^{-1} tetracycline/doxycycline.

Short hairpin RNA. Cells were infected with pLKO-based lentiviral vector with or without the human ASS1 short hairpin RNA (shRNA) encoding one or two separate sequences combined (RHS4533-EG445, GE Healthcare, Dharmacon). Transduced cells were selected with 2 μg ml^{-1} puromycin.

Arginine deprivation combined with drug treatments. U2OS human osteosarcoma cell line was seeded in 6-well plates at 80,000 cells per well. The following day, cells were treated with either 100 nM rapamycin (R0395, Sigma-Aldrich) or with 10 μM 5FU (F6627, Sigma-Aldrich) in regular medium, with 10% dialysed FCS-arginine-free-RPMI (06-1104-34-1A, Biological Industries) or with both arginine-depleted medium and one of these drugs. Rapamycin and 5FU were renewed into the medium every day, whereas fresh arginine-free medium was supplemented twice a week.

Animal studies. According to the approved IACUC protocol 17270415-2, tumours did not exceed the limits of more than 10% of the animal weight and were not longer than 1.5 cm in length in any dimension (Supplementary Fig. 2). Ten million MALME-3m melanoma cells suspended in 500 μl PBS with 5% Matrigel (4132053 Corning) were injected subcutaneously to 8- to 12-week-old male SCID mice that were purchased from Harlan. There were 22 SCID mice, from which 5 or 6 were used for each cell line in each of the three experiments performed. No randomization was used. Mice were monitored for survival and tumour burden twice a week by a veterinarian investigator who was blinded to the expected outcome. Tumours were measured using a calliper. After euthanization, tumours were removed and incubated in medium containing [^{15}N]glutamine for 6 h followed by GC–MS analysis. Tumour size was calculated as published[26].

Building cell models. We used genome-scale metabolic models of NCI-60 cancer cell lines. The reconstruction method (on the basis of methods termed PRIME[10] requires several key inputs: (1) the generic human model[7]; (2) gene expression data for each cell line[19]; and (3) growth rate measurements (available at the NCI website: https://dtp.cancer.gov/discovery_development/nci-60/cell_list.htm). The algorithm then reconstructs a specific metabolic model for each sample by modifying the upper bounds of reactions in accordance with the expression of the individual gene microarray values.

Specifically, the model reconstruction process is as follows. (1) Decompose reversible reactions into unidirectional forward and backward reactions. (2) Evaluate the correlation between the expression of each reaction in the network and the measured growth rate. The expression of a reaction is defined as the mean over the expression of the enzymes catalysing it. (3) Modify upper bounds on reactions demonstrating significant correlation to the growth rate (after correcting for multiple hypothesis using false discovery rate) in a manner that is linearly related to expression value.

***Ass1* probes.** Gcgcatccagggttataagc; gcggagcagggctgagagag; gcccaggcggcagtgg caga; ggccagatgaaccactcagt; agtccgtgtagtctgctttc; gattataggtacaggtccct; ccttgctg gacatcttgtct; ctgtaggccagaaccacaga; gcaggaggtgtccaggccac; gttccttcagccacacgagg; taggcgatgacatcatagcc; cttctggccaatgttggcca; tcctggcttcctcaaagtct; gccccaagcttcag cgcctt; atcctcaatgaacacctttt; cttccacaaattccttgctc; tggacagcaggccagatgaa; gtcctcgta gagtgcactgg; gagaggtgcccaggagatag; cgagctatgcaaggcctggc; ctgggcaatctccacct gtc; acacatacttggccccttca; ccctttcccgtggcgccgtg; ctcaaagcggacctggtcat; gtgccagt gaatagcaggtg; ggagcgatgaccttaatctg; tgtaaaactcaggcatcctc; atcatttcggccccttgaacc; gttgctttgcatactccatc; gtgacagggatggggattcc; catactccaggggctcttgg; tgatgtgcatgag gttttca; tccaggatcccagcctcata; aggtgcttgattcttggggt; gagtttttgtgtagagaccc; ttgg gtgctttggcagggtc; tatctcaaggacatctgggc; cagggaccccttttttgaat; tctttgatgttggtcacctt; ggatgtggtgcgggttgtgc; tcaggtacatgaagagttcc; ccgtgcttgcccgcaacttc; cacgatgtcaatg cgaccca; tcattccaatgaagcggttc; gtctcgtagatacctcggga; gtaaaggatggtccctgctg; cctc tatgtctaaatgagcg; acttcccgatccatcgtgaa; caggccctgcttgatt; cgagctctgcgaatttgagg; ctgtgccagaaacctgtgta; gcgaacaaattcacattcag; cctgggacttctggatacag; tgcaccttcccttc tacccg; ttggcccttgaagacagaca; actcccgaccgaggatgtac; tcattgtagagtgaaagtgg; tgcacgt tcatgctcaccag; gtcgatgggctcatagtcgc; tgatattgatgaagccagtg; tactccttcagcctgagcga; gaccttgctctgaaggcgat; ttgtcagggtctatttggca; gagtggggaggcccgctcct; gctgaagcctggga gagctg; caaatttatcacaacaatta; ggtggagaacaagctacaat; gacacagcagccccagtcag; aggctgt gggggggcggggg; gctatggggaccagggaac; ccttggatgaccacttttgt; agctgcccgccaccctccct; attgtcattttatgctttct; aagactaatgtaacttcttt.

Statistics. All statistical analyses were performed using Tukey's honest significant difference test or independent-samples Student's *t*-test of multiple or two groups, respectively. Log-transformed data were used where differences in variance were significant and variances were correlated with means. The sample size was chosen in advance on the basis of common practice of the described experiment and is mentioned for each experiment. No statistical methods were used to predetermine sample size. Each experiment was conducted with biological and technical replicates and repeated at least three times unless specified otherwise. On the basis of pre-established criteria, individual outlier data points that were more than 2 standard deviations away from the mean were excluded from the data analysis. Statistical tests were done using Statsoft's STATISTICA, version 10. All error bars are standard errors. $P < 0.05$ was considered significant in all analyses ($^*P < 0.05$, $^{**}P < 0.005$, $^{***}P < 0.0005$).

Kaplan–Meier. For each cancer type, the Kaplan–Meier plot indicates the survival rates of the four different groups of patients as labelled. We analysed the cancer types for which there were sufficient survival data.

16. Folger, O. *et al.* Predicting selective drug targets in cancer through metabolic networks. *Mol. Syst. Biol.* **7,** 501 (2011).
17. Varma, A. P. & Palsson, B. O. Metabolic flux balancing: basic concepts, scientific and practical use. *Nature Biotechnol.* **12,** 994–998 (1994).
18. Bordel, S., Agren, R. & Nielsen, J. Sampling the solution space in genome-scale metabolic networks reveals transcriptional regulation in key enzymes. *PLOS Comput. Biol.* **6,** e1000859 (2010).
19. Lee, J. K. *et al.* A strategy for predicting the chemosensitivity of human cancers and its application to drug discovery. *Proc. Natl Acad. Sci. USA* **104,** 13086–13091 (2007).
20. Itzkovitz, S. *et al.* Single-molecule transcript counting of stem-cell markers in the mouse intestine. *Nature Cell Biol.* **14,** 106–114 (2012).
21. Gu, G. J. *et al.* Protein tag-mediated conjugation of oligonucleotides to recombinant affinity binders for proximity ligation. *New Biotechnol.* **30,** 144–152 (2013).
22. Hao, G., Xie, L. & Gross, S. S. Argininosuccinate synthetase is reversibly inactivated by *S*-nitrosylation *in vitro* and *in vivo*. *J. Biol. Chem.* **279,** 36192–36200 (2004).
23. Bjorklund, N. L., Sadagoparamanujam, V. M. & Taglialatela, G. Selective, quantitative measurement of releasable synaptic zinc in human autopsy hippocampal brain tissue from Alzheimer's disease patients. *J. Neurosci. Methods* **203,** 146–151 (2012).
24. Robitaille, A. M. *et al.* Quantitative phosphoproteomics reveal mTORC1 activates de novo pyrimidine synthesis. *Science* **339,** 1320–1323 (2013).
25. Zhang, Y. *et al.* Signal transduction pathways involved in phosphorylation and activation of p70S6K following exposure to UVA irradiation. *J. Biol. Chem.* **276,** 20913–20923 (2001).
26. Pinthus, J. H. *et al.* WISH-PC2: a unique xenograft model of human prostatic small cell carcinoma. *Cancer Res.* **60,** 6563–6567 (2000).

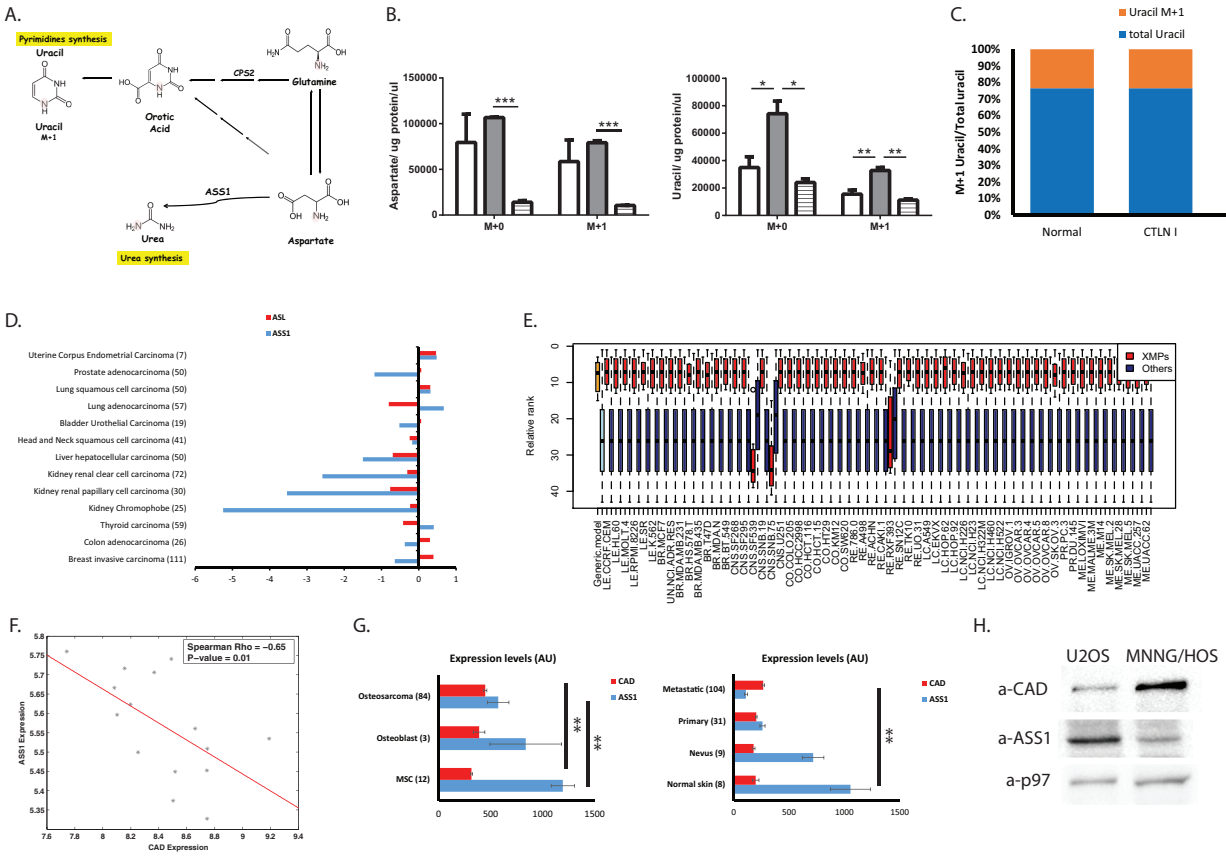

Extended Data Figure 1 | ASS1 deficiency correlates with aspartate utilization by CAD in cancerous and non-cancerous cells. **a**, Schematic flux tracing of the α-labelled nitrogen of glutamine ([^{15}N] α-glutamine) to nucleic acid synthesis via aspartate. **b**, The ratio between M + 1-labelled and total uracil in fibroblasts is similar between patients with citrullinaemia patients and control subjects ($n \geq 3$). Error bars are standard error. **c**, Labelled levels of M + 1 aspartate (left) and M + 1 uracil (right) synthesized from [^{15}N]α-glutamine are higher in fibroblasts from CTLN I than in fibroblasts from controls and patients with CTLN II ($n \geq 3$). **d**, TCGA analysis of tumour–normal paired tissues for gene expression comparison shows the expression levels of *ASL* and *ASS1* in different cancers. **e**, Plot generated from the modelling data for the production capacity of metabolites after ASS1 inactivation in each of the NCI-60 cell lines as well as in the generic model. The reddish bars represent the ranking of nucleic acids while the blueish bars represent the ranking of all other metabolites. **f**, Correlation analysis of NCI-60 cell lines shows a significant inverse correlation between *ASS1* and *CAD* expression levels. **g**, Osteosarcoma (upper) and melanoma (lower) microarray data was obtained from the NCBI EO database (accession numbers GSE33383 and GSE46517, respectively). Raw expression levels were plotted and significance was computed using a *t*-test on $\log_2$-transformed expression levels. The number of patients for each subtype is shown in parenthesis on the left. **h**, Western blot for CAD and ASS1 shows higher expression levels of CAD in the MNNG/HOS human osteosarcoma cell line, which has a low expression level of ASS1 compared with U2OS, which has higher expression levels of ASS1; p97 is shown as loading control.

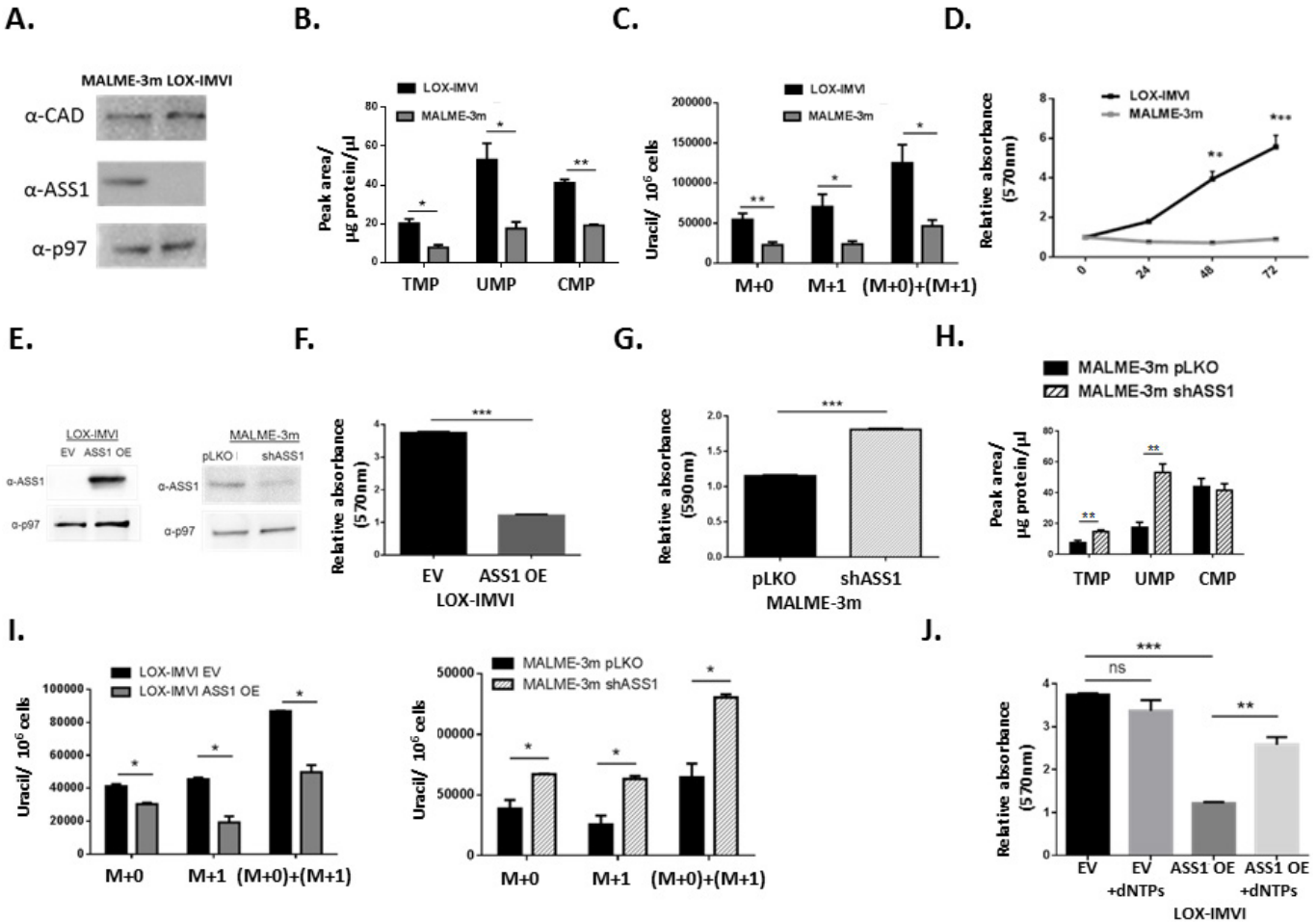

Extended Data Figure 2 | ASS1 inactivation in melanoma correlates with increased proliferation. a, An immunoblot showing different expression levels of ASS1 and CAD in two different cancer cell lines of melanoma. **b**, Melanoma cells with ASS1 downregulation have a significant increase in pyrimidine levels as measured by LC–MS ($n \geq 3$). **c**, Melanoma cells with ASS1 downregulation have a significant increase in total uracil ($n = 4$). **d**, Melanoma cells with ASS1 downregulation have a significant increase in proliferation as measured by MTT assay ($n = 2$). **e**, Immunoblots of melanoma cells for ASS1 levels after transduction with either ASS1 over expression construct or with *shASS1*. **f**, Proliferation assays showing a significant decrease in proliferation after ASS1 overexpression in melanoma using MTT ($n = 3$). **g**, Crystal violet quantification for melanoma cells after transduction with *shASS1* demonstrating increase in proliferation ($n = 3$). **h**, LC–MS measurements of pyrimidine levels showing a significant increase after the use of *shASS1* in melanoma cells ($n \geq 3$). **i**, Left: total uracil levels are decreased significantly in melanoma cells with ASS1 overexpression and increased in melanoma cells with *shASS1* (right) ($n \geq 2$). **j**, Significant increase in proliferation of melanoma cells by dNTPs after ASS1 overexpression ($n = 3$). All error bars are standard errors.

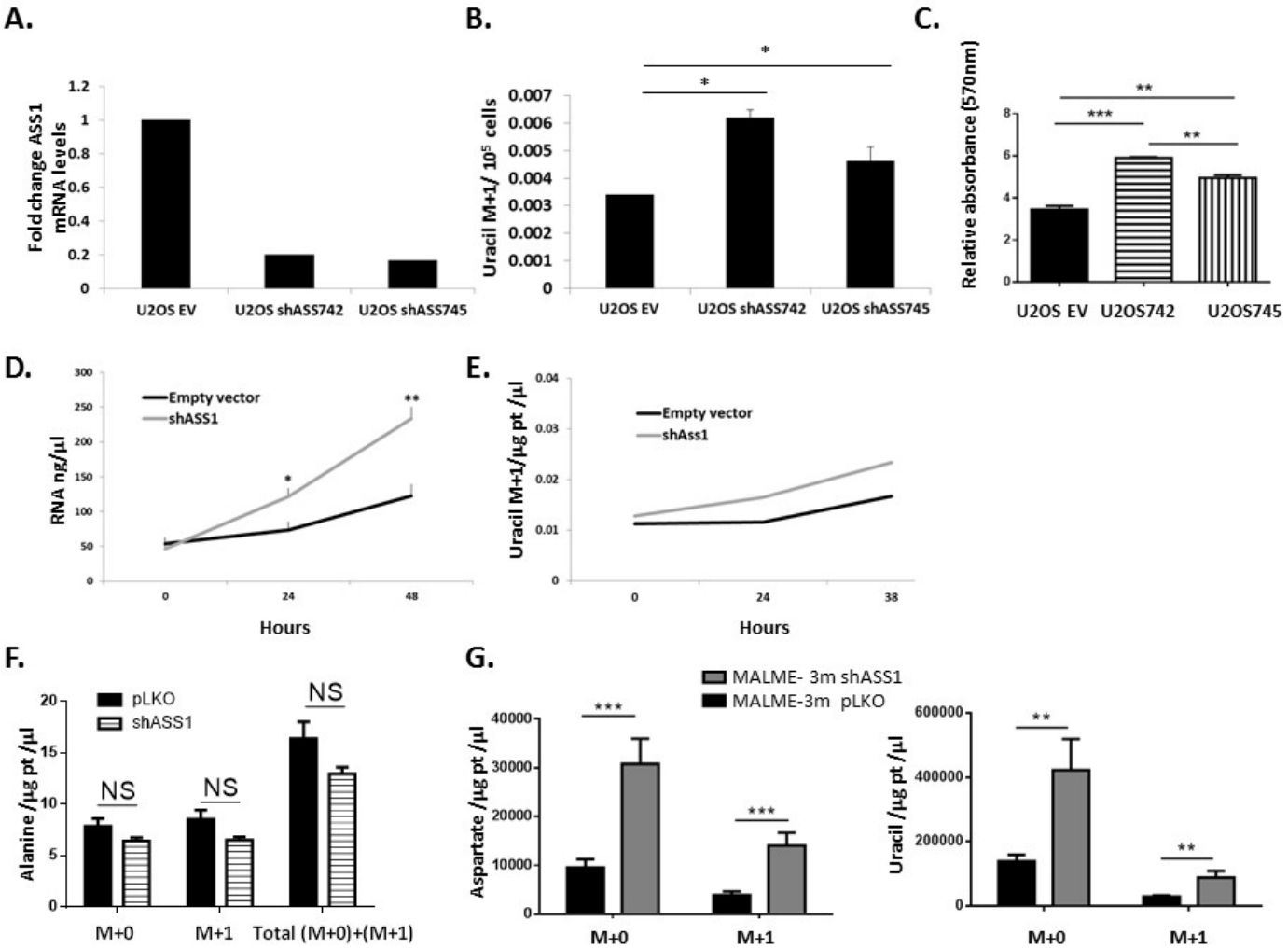

Extended Data Figure 3 | Downregulation of ASS1 levels increases pyrimidine synthesis. a, Osteosarcoma cells were transduced with two different *shASS1* vectors: shASS742 and shASS745. Both clones decreased ASS1 levels efficiently to approximately 20% expression (left), resulting in a significant increase in uracil M + 1 levels (**b**) and in proliferation ($n \geq 3$) (**c**). **d**, RNA levels measured in U2OS at 24 h intervals show increased levels of RNA in U2OS infected with shASS1 compared with the empty vector. **e**, Uracil M + 1 levels increase more in U2OS infected with *shASS1* compared with the empty vector during 38 h of measurements. **f**, The levels of total and labelled M + 1 alanine synthesis from [^{15}N]α-glutamine do not change significantly after ASS1 downregulation ($n = 3$). **g**, Tumours with shASS1 had higher levels of M + 1 aspartate (left) and M + 1 uracil (right) synthesized from [^{15}N]α-glutamine, compared with tumours expressing the empty vector ($n = 15$). All error bars are standard errors.

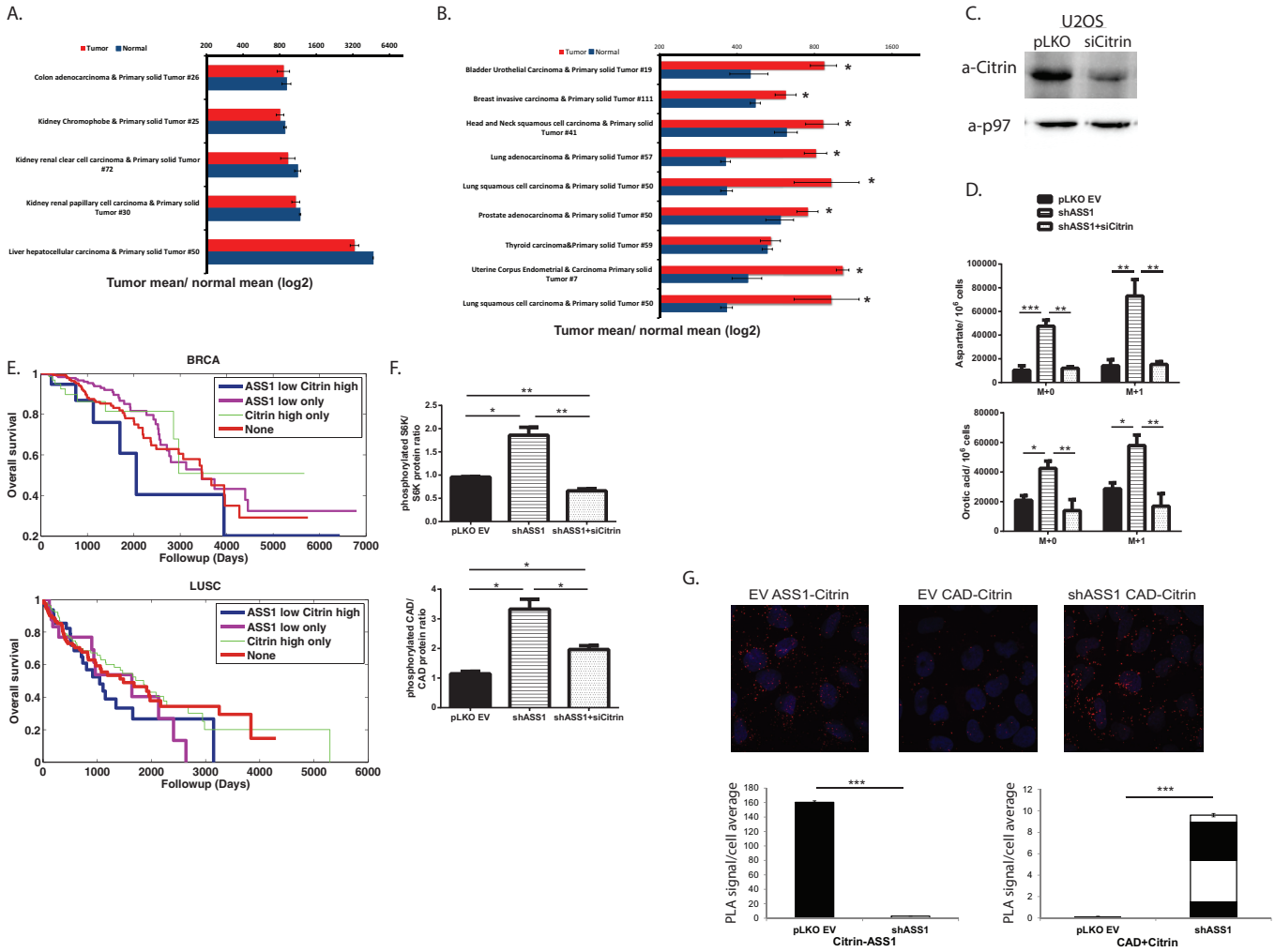

Extended Data Figure 4 | Cancers with ASS1 downregulation are addicted to aspartate. a, **b**, Analysis of the TCGA database of matched tumour–normal pairs showing no significant difference in the expression level of *citrin* in tissues with a high baseline expression of *citrin* (**a**) and significant elevation in tumours in which the normal tissue has low basal expression of *citrin* (**b**) (*$P < 0.001$). **c**, Immunoblot showing the expression level of citrin in osteosarcoma cells after *si-citrin*. **d**, Labelled and unlabelled aspartate (top) and uracil (bottom) are elevated significantly in cancers with ASS1 downregulation and are comparable to control in cells with both ASS1 and citrin downregulation ($n \geq 3$). Error bars are standard errors. **e**, Kaplan–Meier survival analysis for two different cancer types (BRCA, breast cancer (top); LUSC, lung squamous cell carcinoma (bottom)), showing poor survival trend for cancers with low ASS1 and high citrin. For each cancer type, the Kaplan–Meier plot indicates the survival rates of four groups of patients: (1) ASS1 low expression and citrin high expression; (2) ASS1 low expression; (3) citrin high expression; (4) none of these. We analysed the cancer types for which there were sufficient survival data. **f**, Quantification graph of a western blot showing decreased CAD and S6K phosphorylation after treatment of U2OS with *si-citrin*. Error bars are standard errors. **g**, Proximity ligation assay showing increased proximity between CAD and citrin after ASS1 knockdown in U2OS cells (top, red dots). The left and middle pictures show the proximity between ASS1 and CAD to citrin in U2OS infected with empty vector, whereas the right picture shows the proximity between CAD and citrin after infection of U2OS with shASS1. Bottom: quantification of proximity ligation assays performed on U2OS infected with either empty vector (EV) or with *shASS1* using antibodies for citrin, ASS1 and CAD. The pictures were quantified using ImageJ.

Extended Data Table 1 | ASS1 inactivation is predicted to increase aspartate flux for nucleic acid synthesis

Aspartate			
Metabolic Pathway	**Catalyzing Enzymes**	**Inactive ASS1/Active ASS1**	**P-value**
Pyrimidine Biosynthesis	(790.1), CAD	↑	8.47E-198
IMP Biosynthesis	(10606.1) PAICS	↑	<1e-300
Nucleotides	(159.1) Adenylosuccinate synthase	↑	1.55E-265

Predicted fold-change in flux rates through pathways associated with aspartate and glutamine, when comparing ASS1 inactivation with activation state. The most significant change is predicted to effect the pyrimidine biosynthesis pathway followed by purine synthesis pathway (two-sided Wilcoxon rank-sum P value $< 8.4 \times 10^{-198}$, Methods).

Extended Data Table 2 | Kaplan–Meier log-rank data analysis shows significant worsening in the survival of patients with low ASS1 and high citrin expression levels in bladder cancer and lung adenocarcinoma

BLCA		Number of patients	ASS1 low only	Citrin high only	None
	ASS1 low Citrin high	26	0.062029244	0.41802416	0.002920577
	ASS1 low only	437	0	0.939396939	0.133262071
	Citrin high only	83	0	0	0.397997761
	None	415			
BRCA		Number of patients	ASS1 low only	Citrin high only	None
	ASS1 low Citrin high	25	0.091470414	0.348538412	0.215689269
	ASS1 low only	76	0	0.513641931	0.247876216
	Citrin high only	14	0	0	0.784222648
	None	90			
LUAD		Number of patients	ASS1 low only	Citrin high only	None
	ASS1 low Citrin high	34	0.086250611	0.000771207	0.005978456
	ASS1 low only	16	0	0.989469401	0.778260123
	Citrin high only	181	0	0	0.440612674
	None	189			
LUSC		Number of patients	ASS1 low only	Citrin high only	None
	ASS1 low Citrin high	56	0.889254024	0.131597923	0.271250284
	ASS1 low only	35	0	0.234416519	0.540649678
	Citrin high only	173	0	0	0.710240332
	None	127			

The table shows the number of patients for whom data were available in each group, as well as the pairwise *P* value of comparison between the corresponding groups: BLCA, BRCA, LUAD, LUSC.